

#### Sigma Journal of Engineering and Natural Sciences

Web page info: https://sigma.yildiz.edu.tr DOI: 10.14744/sigma.2024.00154



# **Research Article**

# Heat generation from 32650 cylindrical cell battery pack at various load and speed conditions

Shashank GAWADE<sup>1,2,\*</sup>, Virendra BHOJWANI<sup>2</sup>, Pradeep PATIL<sup>1</sup>, M. ZUBAIRUDDIN<sup>3</sup>

<sup>1</sup>Jayawantrao Sawant College of Engineering, Pune, 411028, India <sup>2</sup>MIT ADT University, Pune, 412201, India <sup>3</sup>Aditya University, Surampalem, 533003, India

#### **ARTICLE INFO**

Article history
Received: 13 July 2024
Revised: 21 August 2024
Accepted: 25 October 2024

#### **Keywords:**

Electric Vehicles; Heat Generation; Joule's Heat; LiFePO<sub>4</sub>

#### **ABSTRACT**

Electric vehicles are penetrating the transportation sector with a pace to reduce greenhouse gases and climate changes. Some limitations to penetrating in market are range, thermal performance, and battery cost. The performance of electric vehicles is majorly based on the quality and chemistry of the battery. The current study is on the Lithium Iron Phosphate battery pack of 48 V 42Ah with an ambient temperature. The current demand for electric vehicles varies with the speed under various loading conditions. Heating of the battery in real-time is one of the problems currently faced by automakers. The Joule's heat is the primary parameter for increasing the battery's temperature. Prediction of the heat generation in the battery was carried out with different mechanisms at constant charge/discharge rate, not with dynamic loading. The inefficient battery thermal management system may result in the thermal runaway, leading to fire catch incidents, hence estimation of the current withdrawal needs to be accurate. To predict heat generation, 1. Bernardi's equation used, but having limitation in predicting accurate heat prediction, 2. Ohmic/Joule's equation, the current must be known. Hence, experiments carried out to find the current withdrawal under different actual loading conditions. In this work, the temperature rise under various loading conditions is measured on the single-wheel vehicle model operated on a battery, at varying conditions of rolling resistance, load, speed, and test duration. Experiment results show a 7.6 & 6.7°C rise in battery temperature at 125 kg, 15km/hr speed for 75 min on concrete and tar roads, respectively. From the experimental result need of the battery thermal management system, heat dissipation rate can be efficiently designed.

Cite this article as: Gawade S, Bhojwani V, Patil P, Zubairuddin M. Heat generation from 32650 cylindrical cell battery pack at various load and speed conditions. Sigma J Eng Nat Sci 2025;43(6):1–13.

This paper was recommended for publication in revised form by Editor-in-Chief Ahmet Selim Dalkilic



<sup>\*</sup>Corresponding author.

<sup>\*</sup>E-mail address: ssgawade24@gmail.com

#### INTRODUCTION

Conventional internal combustion engine (ICE) vehicles have limitations of harmful emissions, limited fossil fuel sources, and high transportation cost per kilometer. Conventional ICE vehicles are being replaced by electric vehicles (EVs) which use rechargeable batteries as a source of energy, a motor, and a controller. In the global market, the share of EVs in the automotive market has significantly increased in the last decade. Furthermore, extensive research in battery technology has remarkably decreased battery costs, resulting in a market share. Worldwide efforts are to improve the performance of EV batteries and the vehicle's performance. During the battery discharge, the cells used for battery construction generate a significant amount of heat, which causes a rise in the battery pack's temperature.

While the literature survey provides valuable insights into the heat generated in the cell at the laboratory level during constant current discharge, it also reveals a significant gap in our understanding. There are very few papers that delve into the current withdrawn from the battery at various speeds, under different payloads, and in different road conditions. These factors, such as rolling resistance, payload, and vehicle speed, can significantly vary the power demand at different intervals. This scarcity of literature underscores the urgency of further research in this area to ensure the optimal performance and safety of EV batteries under real-world conditions.

Lithium Iron Phosphate (LFP), Lithium Nickel-Cobalt-Aluminum Oxide (NCA), and Lithium-Nickel-Manganese-Cobalt-Oxide (NMC) batteries were experimentally tested at ambient temperature and under different operating currents, measuring cell voltage and surface temperature [1]. The elevated temperature affects the battery's performance, causing capacity fade, fire hazards, thermal runaway, etc [2]. Thermal runaway occurs when the cell's temperature is over the working temperature due to the heat-generating reactions within the cell, causing flammable gasses [3]. One impact of the cell's increase in temperature occurred on the battery's SoC estimation. SoC determines the present current density of the battery [4]. During the discharging of the cell, the heat evolved inside the cell, which causes the SEI layer to decompose, binder decomposition, enhance the rate of reaction, and decomposition of the electrolyte, which results in the gas buildup inside the cell [5].

A battery thermal management system was adopted to limit the temperature rise of the battery pack. Several thermal management techniques include air cooling systems, liquid cooling systems, phase change materials, composite phase change materials, etc. The selection of a suitable thermal management system depends on the heat generated in the battery pack. Hence, estimating the amount of heat generated in the battery pack is crucial in deciding the type of thermal management system. Researchers continuously develop battery thermal management systems (BTMS)

by adopting different approaches. Few authors developed novel BTMS for Lithium-ion batteries (LIBs) employing air cooling strategies like symmetrical air-cooling, two-directional air-flow approach, air cooling coupled to water evaporation, and metal and non-metal foams [6-12]. Liquid excellent BTMS technique was studied extensively by various researchers [13], where coolants like water, Nanofluid, and water-ethylene glycol mixture, along with novel techniques/arrangements like micro-vascular composites, mini-channel aluminium tubes, circuitous channels, etc., were studied. In addition to this, researchers have investigated BTMS employing novel techniques using phase change materials (PCM), composite phase change materials (CPCM), and heat-pipe approach [11-18]. Hybrid cooling mechanism, where air and liquid cooling are adopted for efficient cooling [19]. Paraffin wax, along with Al<sub>2</sub>O<sub>3</sub> Nanoparticles, shows enhancement in the charging and discharging process of the PCM [20]. Fly ash Nanofluid in the base of water-ethylene glycol (ratio 3:1) shows better heat dissipation over the simple water-ethylene glycol (ratio 3:1) as a coolant [3, 21]. Different authors used K-type thermocouples for thermal cycles during different processes [22-24]. The sources of heat generation in the LIB's are reversible heat generation and irreversible heat generation due to activation, concentration, and ohmic (electronic and ionic) polarizations – in with graphite/LiFePO<sub>4</sub> electrode materials [25]. One of the most used methods to measure the heat generated in the cell is the accelerating rate calorimeter (ARC), restricted to use under adiabatic conditions and for the high rate operating cells [26]. Allouhi et al. proposes the design of an electricity charging station for small-size electric vehicles powered by the same HRES. It help Moroccan authorities to have insight on the role that can play HRES systems to not only enhance the energy efficiency of supermarkets and lower their emissions but also how they can help in transitioning towards a clean and green mobility [27]. The lithium-ion batteries get affected due to the high temperature in view of safety and performance. Due to high temperatures side reactions occurred result to degradation of cell capacity and the fading of electrochemical performance [26]. Artificial intelligence and machine learning techniques show a promising future to predict the current withdrawal from the past data set [28].

In this work, an attempt is made to investigate the effect of the loading condition on the heat generated in the Lithium Iron Phosphate (LFP) cell. During real-time driving, the speed and payload on the vehicle vary which causes changes in the power demand and current demand from the battery. Currently, in the literature survey, the heat generated at the constant current output was discussed at different loading conditions. The experiment study gives the relationship of the current withdrawn from the battery with respect to the payload, rolling resistance, and speed of the vehicle. As the Joules heat, the major parameter to raise the temperature inside the battery solely depends on the withdrawn current. This study predicts the current withdrawal

and heat generated in the battery under different loading conditions. Depending on the battery's heat generated, the battery thermal management system's deployment can be easily selected. To evaluate the performance of the battery pack, a single wheel was tested using a test dynamometer at different load and speed conditions.

#### Heat Generation in the Cell

In the present study, lithium iron phosphate (LFP) type lithium-ion battery cells are investigated. The LFP cells use LiFePO $_4$  as a cathode material, while a form of carbon is an anode material. The lithium ions (Li<sup>+</sup>) travel from the anode to the cathode through the electrolyte during the cell discharge and from the cathode to the anode during the cell charge. These ions get rapidly integrated into the cathode material once they reach the cathode. The charge and discharge reactions in the battery are presented in Eq.1 and 2, respectively [13].

Charge reactions:

$$FePO_4 + xLi^+ + xe^- = xLiFePO_4 + (1-x) FePO_4$$
 (1)

Discharge reactions:

$$LiFePO_4 - xLi^+ - xe^- xFePO_4 + (1-x) LiFePO_4$$
 (2)

The estimation of heat generation in the cell during the charge and discharge process is vital to deciding on the type of battery thermal management system for the battery pack. To estimate the heat generation within the battery cell, it is crucial to understand the mechanism of heat generation have mentioned various approaches for measuring the battery heat generation (1) through direct experimental tests, (2) by employing Bernardi's equations, and (3) by adopting electro-thermal coupling model. Predicting heat generation within the battery using the Bernardi equation is a highly effective, time-saving approach with equitable results [13].

In the LFP cell, heat generation is primarily due to polarization heat, heat released during chemical reactions, and Joule's heat. Of these, Joule's heat, which is related to Ampere<sup>2</sup> x Internal resistance, is the major contributor to heat generation in the cell. As the load and speed change, the power demand to cope with these conditions increases, leading to an increase in current and subsequently, the temperature of the cell.

The Bernardi equation is given below,

$$Qgen = I(U - V) - I \left[ T - \frac{dU}{dT} \right]$$
 (3)

where,  $Q_{gen}$  = the rate of heat generation (W), I = the cell current (A), U = the open circuit voltage (V), T = the temperature (K), and V = the cell terminal voltage (V). The first term of the equation quantifies the heat generation due to the polarization effects in the cell whereas the second term quantifies the entropic heat generation [29-32]. However,

this equation does not consider the heat generation due to the phase change and mixing [33].

The term  $\partial U/\partial T$  which is a derivative of OCV with respect to the temperature is termed as entropic coefficient of the cell.

Accurate estimation of heat generation is critical for EV batteries. Conventional means of heat estimation (i.e., Bernardi equation) work only for constant current discharge. However, fluctuating current conditions are the standard mode of operation for cells in EV applications. It is noted that Bernardi method is an indirect method of heat estimation based majorly on electrical parameters. It is also observed that the reversible part of Bernardi heat is negligible under drive cycle operation. Lithium-ion batteries can utilize various cathode chemistries, including LFP, LCO, and NMC. Each cathode chemistry has distinct advantages and disadvantages concerning specific capacity, energy/power density, cost, and thermal stability [34].

#### **EXPERIMENTAL SETUP AND PROCEDURE**

For the experimental work, four parameters are considered with high priority, Speed of vehicle, Payload on vehicle, Time of drive, and the road surface itself. The coefficient of drag and road gradient were not considered for the study as the coefficient of drag is finalized by the vehicle manufacturer and is independent of the driver. Road gradient, in the urban area, the slope from underground to basement or elevation at the overhead bridge is present by maximum elevation is up to 500 meters, which covers in maximum of 2-3 minutes, so consideration of the same for the whole duration of time was exempted after expert comment.

The payload is an essential parameter of the vehicle. Here two two-wheeler vehicles were considered in the study. In a typical scenario average weight of a single person in India is 68 kg. Considering the vehicle running without a person, only the vehicle's weight plays a critical role. Hence, 80/2 kg was considered for lower-weight conditions. On the higher side, the average weight of the person is multiplied by 2.5 to consider variations in the weight. Furthermore, an additional 80 kg wt. of chassis was added to the calculation for deadweight and safety analysis for extreme variation in weight. All this counted to 250/2 kg as a higher side weight in the analysis.

As per the SAE J2452 standard, the rolling resistance for the tar road is 0.013, and for the concrete, it is 0.01. In urban areas, the roads are constructed with tar or concrete roads; hence, these conditions are implemented with the two Mild steel roads at the bottom of the Tire.

In the Indian context, the diversity in the weight and driving pattern of the driver gender was observed widely. The range of the vehicle majorly depends on the payload of the vehicle. As per observation, the male (age 30 onwards) drives smoothly with experience to gain high performance, whereas the female driving pattern differs from the male in which jerky motion is involved. After benchmarking with

MINITAB software, different payload combinations, time, and speed combinations were formulated with the surface response method.

#### **Battery Pack**

The battery pack of 48-volt 42 Ah is constructed with 32650 (32 mm diameter, 65 mm height of cell & Circular shape) lithium iron phosphate (LFP) cylindrical cell with nominal voltage 3.2 V and 6000 mAh capacity. The battery pack consists of 112 nos. in Two stacks, an upper and lower stack each containing 56 LFP cells. Technical specifications of the cells used for battery construction with battery are tabulated in Table 1. In each stack, the cells are arranged in eight series – seven parallel (8S7P) layout with an effective capacity of 42Ah and a nominal voltage of 24V. The upper and lower stacks are then connected in series to double the nominal voltage of the battery pack to 48V. The battery pack is used to operate an electric two-wheeler. The pictorial view of the battery pack is shown in Figure 1.

**Table 1.** Technical specifications of cell and battery pack

Parameter	Value	Battery pack
Nominal voltage	3.2 V	48 V
Cell capacity	6000 mAh	42 Ah
Diameter	32 mm	
Height	65 mm	
Mass	160 g	17.92 kg
Cut off voltage	2.8 V	
Internal resistance	0.02 ohm	



Figure 1. Battery pack

#### **Experimental Setup**

The objective of this work is to evaluate the temperature rise of the battery pack by measuring the battery cell's temperature during the vehicle's operation. The various operating conditions include rolling resistance, load, speed, and duration of operation. Rolling resistance of 0.01 and 0.013 are selected to simulate the tar and concrete road conditions [35]. With these rolling resistance values, tests were performed at different loads and speeds, as specified in Table 3. A chassis dynamometer test setup was developed to simulate the operating conditions with a single fixed roller. The laboratory setup is depicted in Figure 2. The wheel rolls over the single fixed roller (shaft) at various speeds through a chain and sprocket mechanism by a motor. The roller shaft is supported over the pillow bearing on the I-section base and is free to rotate. The wheel rotates over a shaft, which applies a rolling resistance to the wheel. The brushless DC motor controller takes power from the battery and supplies it to the motor as per the requirement. A 1 k $\Omega$  potentiometer communicates the power required to the controller based on the accelerator position. A 48V brushless DC motor with a maximum power of 1500 W and a maximum speed of 3000 rpm was used to drive the wheel assembly. The display on the front panel shows the battery voltage and the current. A miniature circuit breaker (MCB) protects the circuit from excessive current during overloading and short circuits.

The payload is an essential parameter of the vehicle. Here two two-wheeler vehicles were considered in the study. In a typical scenario average weight of a single person in India is 68 kg. Considering the vehicle running without a person, then only the weight of the vehicle plays a key role. Hence, 80/2 kg was considered for lower-weight conditions. On the higher side, the average weight of the person is multiplied by 2.5 to consider variations in the weight.

Furthermore, an additional 80 kg wt. of chassis was added to the calculation for deadweight and safety analysis for extreme variation in weight. All this counted to 250/2 kg as a higher side weight in the analysis. In the urban city as per the survey, 80-90% of the population drives a vehicle with 25 km/h speed due to the road, traffic, and signal control conditions, either on the tar road or concrete road.

Figure 2 shows the laboratory test setup with a 35 mm mild steel shaft under the tire to assess rolling resistance conditions. During each test, a data acquisition system records the voltage of the battery pack and the discharge current. To measure the cell's temperature, thermocouples were attached to the surfaces of the different cells in the upper and lower stacks. Type 'T' thermocouples with a temperature inaccuracy of  $\pm 0.75\%$  were used to measure the cell's temperature. A multichannel data logger was used to record the temperature data at fixed intervals. The layout of the battery pack and the location of the thermocouples are depicted in Figure 3. The shaded cells show the location of the thermocouple.

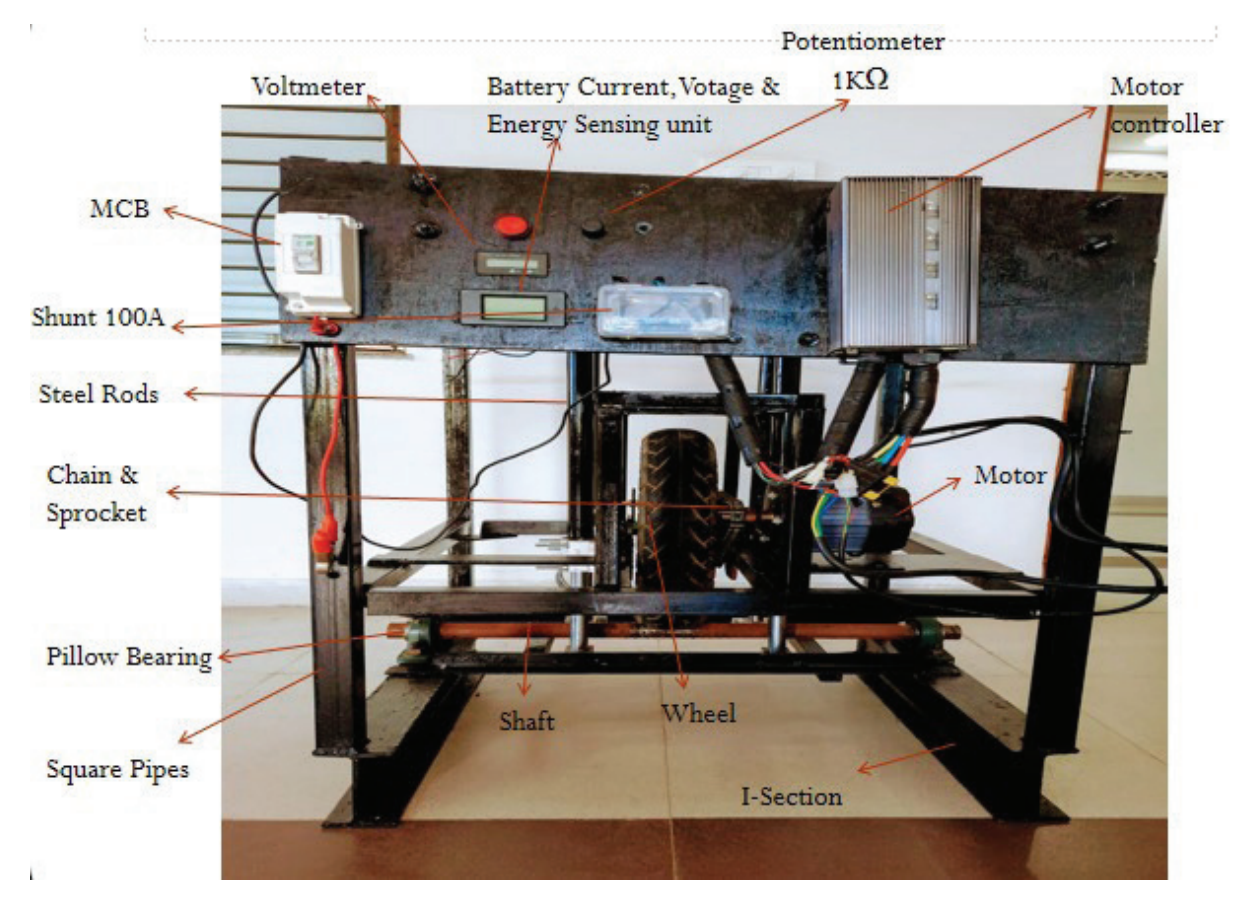


Figure 2. Test setup.

LA <sub>1</sub>	LA <sub>2</sub>	LA <sub>3</sub>	$LA_4$	LA <sub>5</sub>	LA <sub>6</sub>	LA <sub>7</sub>
LB <sub>1</sub>	LB <sub>2</sub>	LB <sub>3</sub>	$LB_4$	LB <sub>5</sub>	LB <sub>6</sub>	LB <sub>7</sub>
$LC_1$	$LC_2$	LC <sub>3</sub>	$LC_4$	LC <sub>5</sub>	LC <sub>6</sub>	LC <sub>7</sub>
LD <sub>1</sub>	$LD_2$	LD <sub>3</sub>	$LD_4$	LD <sub>5</sub>	LD <sub>6</sub>	LD <sub>7</sub>
LE <sub>1</sub>	LE <sub>2</sub>	LE <sub>3</sub>	LE <sub>4</sub>	LE <sub>5</sub>	LE <sub>6</sub>	LE <sub>7</sub>
LF <sub>1</sub>	LF <sub>2</sub>	LF <sub>3</sub>	LF <sub>4</sub>	LF <sub>5</sub>	LF <sub>6</sub>	LF <sub>7</sub>
LG <sub>1</sub>	$LG_2$	LG <sub>3</sub>	LG <sub>4</sub>	LG <sub>5</sub>	LG <sub>6</sub>	LG <sub>7</sub>
LH <sub>1</sub>	LH <sub>2</sub>	LH <sub>3</sub>	LH <sub>4</sub>	LH <sub>5</sub>	LH <sub>6</sub>	LH <sub>7</sub>

UA <sub>1</sub>	UA <sub>2</sub>	UA <sub>3</sub>	UA <sub>4</sub>	UA <sub>5</sub>	UA <sub>6</sub>	UA <sub>7</sub>
$UB_1$	UB <sub>2</sub>	$UB_3$	UB <sub>4</sub>	UB <sub>5</sub>	UB <sub>6</sub>	UB <sub>7</sub>
$UC_1$	$UC_2$	UC <sub>3</sub>	$UC_4$	UC <sub>5</sub>	$UC_6$	UC <sub>7</sub>
$UD_1$	$UD_2$	$UD_3$	UD <sub>4</sub>	$UD_5$	$UD_6$	UD <sub>7</sub>
UE <sub>1</sub>	UE <sub>2</sub>	UE <sub>3</sub>	UE <sub>4</sub>	UE <sub>5</sub>	UE <sub>6</sub>	UE <sub>7</sub>
UF <sub>1</sub>	UF <sub>2</sub>	UF <sub>3</sub>	UF <sub>4</sub>	UF <sub>5</sub>	UF <sub>6</sub>	UF <sub>7</sub>
$UG_1$	UG <sub>2</sub>	$UG_3$	$UG_4$	$UG_5$	UG <sub>6</sub>	UG <sub>7</sub>
UH <sub>1</sub>	$UH_2$	$UH_3$	$UH_4$	$UH_5$	UH <sub>6</sub>	UH <sub>7</sub>

(a) Upper Stack (b) Lower Stack

**Figure 3.** Layout of battery pack and location of thermocouples.

Since each cell in the battery pack is subjected to the varying conditions of the convection, it is vital to measure the temperature of cells at various locations. To differentiate it, the cells in the battery pack are classified into regions as layer 1 (L1), layer 2 (L2), layer 3 (L3), and layer 4 (L4). Layer 1 includes the cell in the outermost

region of the battery pack directly exposed to atmospheric air. Layer 2 includes the cells in the layer inside r 1, and layer 3 includes the cells inside r 4 in the core central part of the battery pack. Table 2 lists cells with thermocouples in each layer of the battery pack for the upper and lower stack.

Table 2. Thermocouples in different regions of battery pack

Region	Upper Stack	Lower Stack
L1	UA1, UA7, UH1, UH7	LA1, LA7, LH1, LH7
L2	UB2, UB6, UG2, UG6	LB2, LB6, LG2, LG6
L3	UC3, UC5, UF3, UF5	LC3, LC5, LF3, LF5
L4	UD4, UE4	LD4, LE4

# **RESULT AND DISCUSSION**

# **Temperature Rise of Cell**

The heat generated in the battery during the discharge is dissipated to the surrounding air by the convection mode of heat transfer. The heat transfer rate depends upon the ambient temperature heat transfer coefficient and is

**Table 3.** Test specifications

Sr. No.	Parameter	Lower value	Higher Value
1	Speed of vehicle (km/h)	05	25
2	Payload (kg)	80/2	$\{[(68x2.5) + 80] = 250\}/2$
3	Rolling resistance coefficient	0.01 for tar	0.013 for concrete
4	Time (minutes)	10	75

**Table 4.** Experimental value

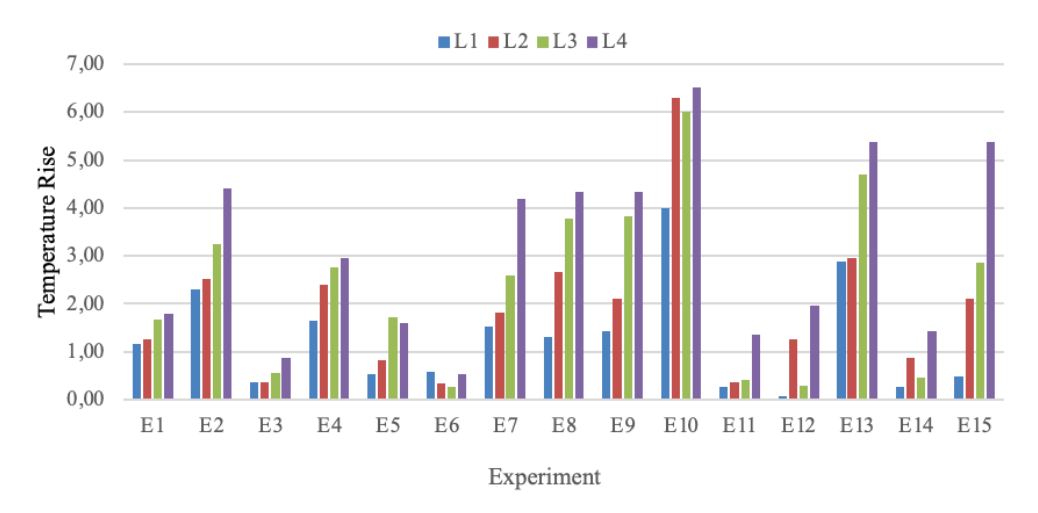
<b>Experiment No.</b>	Designation	Rolling Resistance (RR)	Load (kg)	Speed (km/h)	Duration of Test (min)
1	E1	0.01	40	05	43
2	E2	0.01	82.5	05	75
3	E3	0.01	82.5	05	10
4	E4	0.01	125	05	43
5	E5	0.01	40	15	75
6	E6	0.01	40	15	10
7	E7	0.01	82.5	15	43
8	E8	0.01	82.5	15	43
9	E9	0.01	82.5	15	43
10	E10	0.01	125	15	75
11	E11	0.01	125	15	10
12	E12	0.01	40	25	43
13	E13	0.01	82.5	25	75
14	E14	0.01	82.5	25	10
15	E15	0.01	125	25	43
16	Y1	0.013	40	05	43
17	Y2	0.013	82.5	05	75
18	Y3	0.013	82.5	05	10
19	Y4	0.013	125	05	43
20	Y5	0.013	40	15	75
21	Y6	0.013	40	15	10
22	Y7	0.013	82.5	15	43
23	Y8	0.013	82.5	15	43
24	Y9	0.013	82.5	15	43
25	Y10	0.013	125	15	75
26	Y11	0.013	125	15	10
27	Y12	0.013	40	25	43
28	Y13	0.013	82.5	25	10
29	Y14	0.013	82.5	25	75
30	Y15	0.013	125	25	43

available for the convection. For the battery pack under investigation, the outer cells are exposed to the inner side of the battery pack. However, the cells at the inner locations are subjected to the heated trapped air in the battery pack. As a result, the heat transfer coefficient at the outer cell surface is more significant than that at the inner cells of the battery pack. Consequentially, it is evident that the inner cells are subjected to more extraordinary temperature rise than the outer cells of the battery pack. The average rise in temperature of cells in each region battery pack for all tests with rolling resistance of 0.01 and 0.013 are shown in Figure 4 a and b, respectively.

It is perceptible that the average rise in temperature of cells in the core region of the battery (L4) is more significant than all other layers, followed by regions L3, L2, and L1. The average temperature rise for the region L1 is lower than the other regions due to the higher convective coefficient. As ambient air enters the battery pack, it gets heated by heat generation in the cells, reducing the heat transfer rate from the cell to the air in the battery pack's central part. Because of this, the temperature rise in the L4 region of the battery is higher than in other regions.

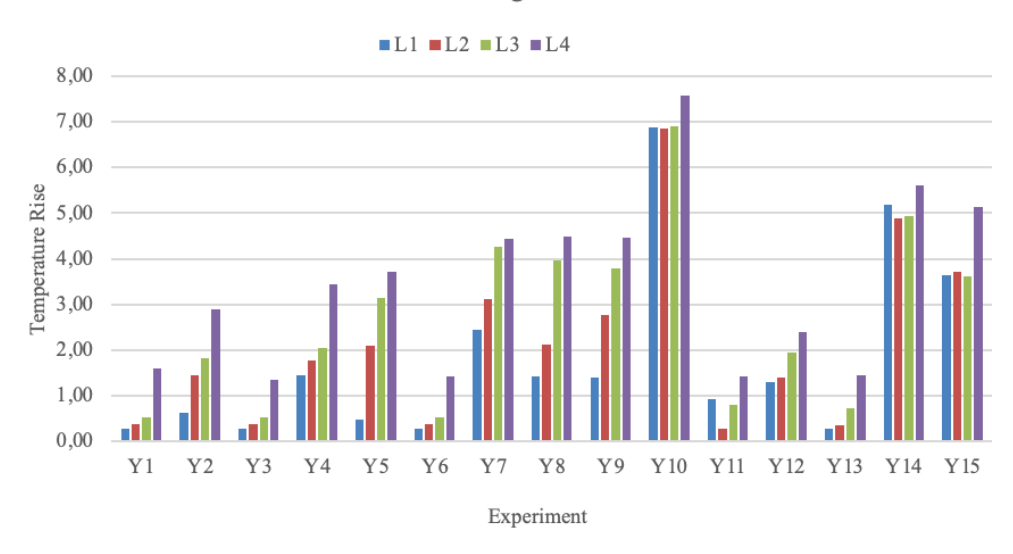
The cells in the central part of the battery pack experience a lower heat dissipation rate, leading to a higher cell temperature than cells in other parts of the battery pack.

# 0.01 Rolling Resistance



#### a) For Rolling Resistance 0.01

# 0.013 Rolling Resistance



# b) For Rolling Resistance 0.013

Figure 4. The average rise in temperature of cells in each region of the battery pack.

<b>Table 4.</b> Maximum temperature rise of the battery
---

Test	Maximum temperature rise	Test	Maximum temperature rise
E1	1.9	Y1	1.7
E2	4.5	Y2	3.1
E3	0.9	Y3	0.9
E4	3.3	Y4	3.5
E5	3.2	Y5	3.8
E6	1	Y6	1
E7	4.3	Y7	4.5
E8	4.5	Y8	4.7
E9	4.4	Y9	4.6
E10	6.7	Y10	7.6
E11	1.4	Y11	1.5
E12	2.1	Y12	2.4
E13	5.4	Y13	1.6
E14	1.5	Y14	5.7
E15	5.6	Y15	5.3

For all other cells, a portion of the heat generated by the cell is dissipated to the atmospheric air through the convection plus conduction mode of heat transfer. The cell surface temperature is crucial to measuring the entropic heat generation in the battery pack accurately. For this purpose, the maximum temperature rise of the cell is considered for each test. The maximum temperature rise of the battery pack for each test is detailed in Table 4.

# Effect of Load on Maximum Temperature Rise

The experimental tests are conducted at varying loads, speeds, and test times. The effect of load on maximum temperature rise for various test conditions is exhibited in the graphical form in Figure 5. As the load increases from 40 to 125 kg, the temperature-increased behavior was observed at 05, 15 & 25 km/for 43, 75 & 43 minutes, respectively.

# Temperature Rise at Varying Loads

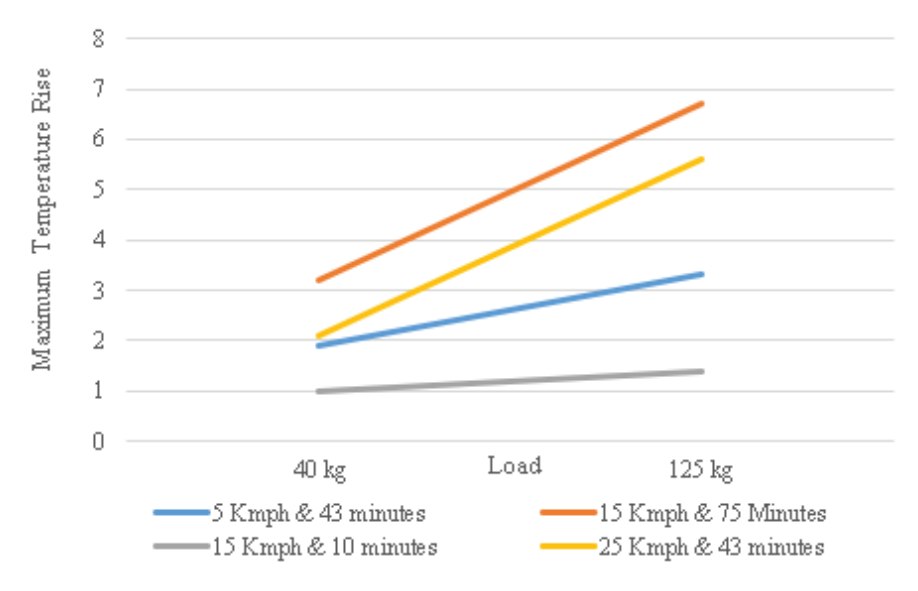


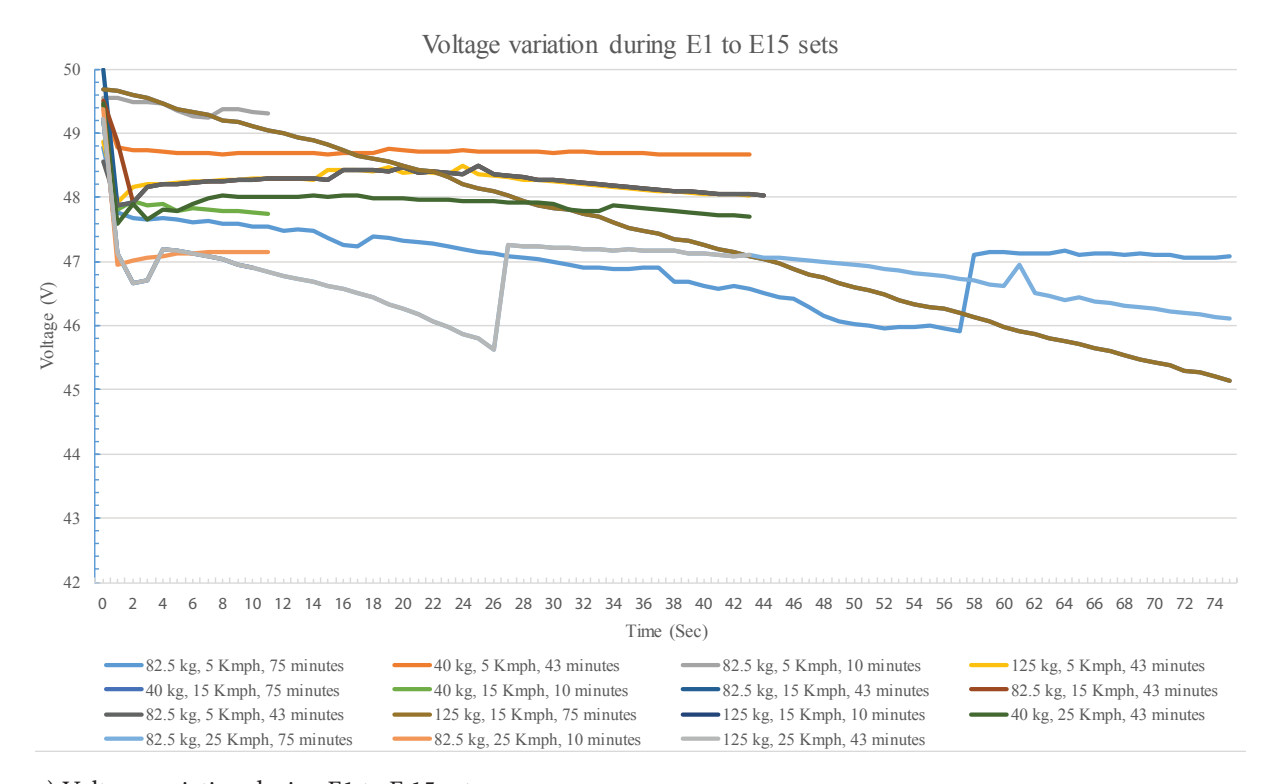
**Figure 5.** Temperature rise at varying loads.

# **Heat Generation Per Minute Under Different Loading Conditions**

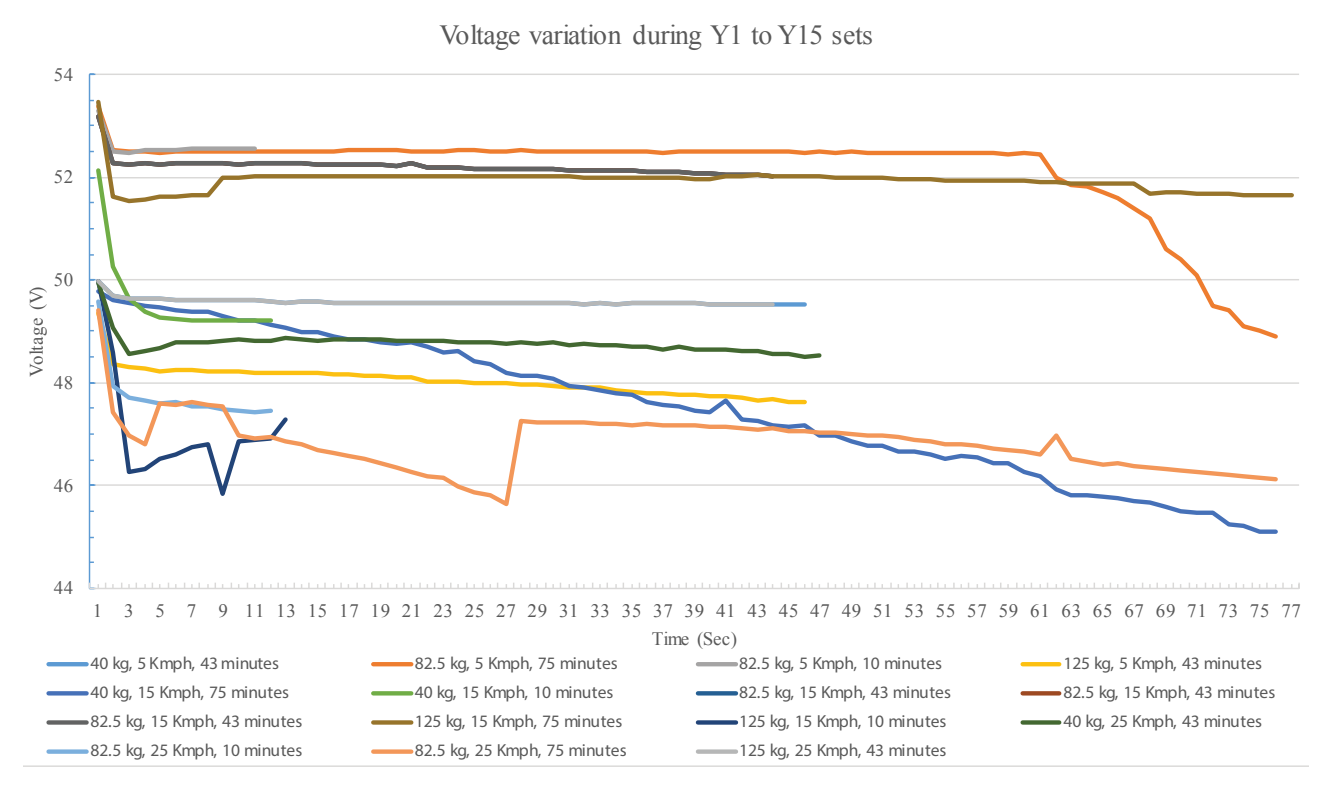
The voltage and current delivered by the battery pack and the cells' surface temperature were recorded during the test. The time-dependent current and voltage values are required to estimate the heat generation in the battery pack using the Bernardi theoretical model. The value of current and voltage values with time are shown in Figure 6 (a- ad). The rate of heat generation during each test is tabulated in Table 5.

**Table 5.** Temperature rise per minute for different tests

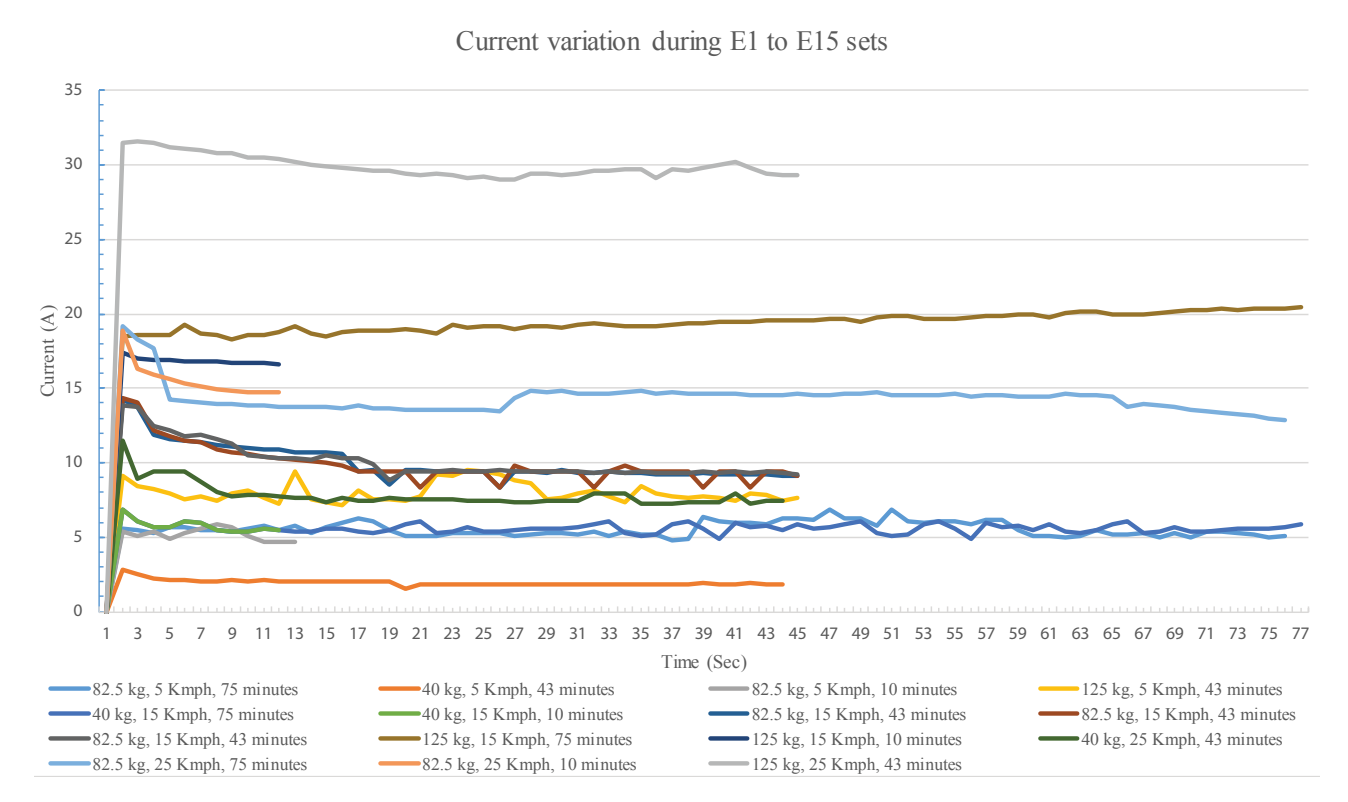
Test	Temperature rise per minute by exp. (°C)	Test	Temperature rise per minute by exp. (°C)
E1	0.67	Y1	0.78
E2	0.77	Y2	0.59
E3	0.18	Y3	0.30
E4	0.39	Y4	0.40
E5	0.60	Y5	0.80
E6	0.17	Y6	0.26
E7	0.41	Y7	0.56
E8	0.42	Y8	0.47
E9	0.41	Y9	0.41
E10	0.33	Y10	0.68
E11	0.07	Y11	0.16
E12	0.22	Y12	0.27
E13	0.28	Y13	0.08
E14	0.08	Y14	0.30
E15	0.20	Y15	0.15



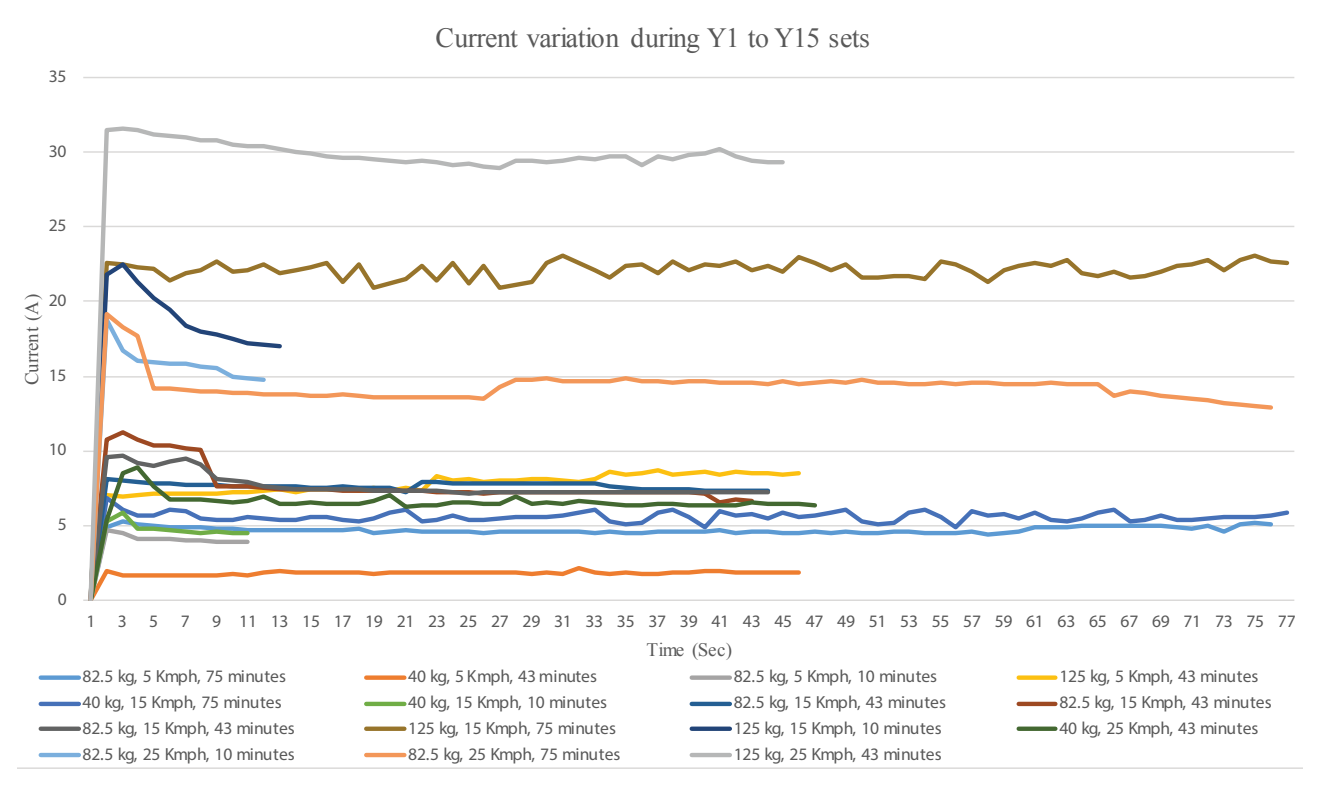
a) Voltage variation during E1 to E 15 sets.



# b) Voltage variation during Y1 to Y 15 sets.



# c) Current variation during E1 to E 15 sets.



d) Current variation during Y1 to Y 15 sets.

Figure 6. Effect on voltage and current at various load and speed

#### CONCLUSION

A single-wheel vehicle model was operated through a battery pack on a test dynamometer at varying rolling resistance, load, speed, and test duration conditions. The battery pack's voltage, current, and temperature were recorded during the test to investigate the temperature rise in the battery. It can be concluded that the temperature rise is within the permissible limit of the Lithium iron phosphate chemistry. So, natural heat dissipation from the cell's surface is sufficient to keep the cell in the working temperature range. The experiment study also discussed the relationship of the current withdrawn from the battery concerning the payload, rolling resistance, and speed of the vehicle. As the Joules heat, the major parameter to raise the temperature inside the battery solely depends on the withdrawn current. This study predicts the battery's current withdrawal and heat generated under different loading conditions. Depending on the battery's heat generated, the battery thermal management system's deployment can be easily selected. The following conclusions were drawn from the study.

- For rolling resistance of 0.01, for 125kg, 15 km/h & 75 min, the maximum absolute temperature recorded was 33.2°C with a temperature rise of 6.7°C in comparison to the ambient air at a temp 26.5°C. The maximum temperature of the battery pack is well below the safe operating temperature limits of the cell.
- For rolling resistance of 0.013, for 125kg, 15 km/h & duration of 75 min, the maximum absolute temperature

- recorded was 36.1°C with the temperature rise of 7.6°C in comparison to the ambient air at a temperature 28.5°C. The maximum temperature of the battery pack is well below the safe operating temperature limits of the cell.
- There is no need for a sophisticated active thermal management system to maintain the temperature of the battery pack.
- However, under extreme working conditions, if atmospheric temperature increased above 45°C, it would require a dedicated thermal management system.

# **AUTHORSHIP CONTRIBUTIONS**

Authors equally contributed to this work.

# **DATA AVAILABILITY STATEMENT**

The authors confirm that the data that supports the findings of this study are available within the article. Raw data that support the finding of this study are available from the corresponding author, upon reasonable request.

# **CONFLICT OF INTEREST**

The author declared no potential conflicts of interest with respect to the research, authorship, and/or publication of this article.

#### **ETHICS**

There are no ethical issues with the publication of this manuscript.

# STATEMENT ON THE USE OF ARTIFICIAL INTELLIGENCE

Artificial intelligence was not used in the preparation of the article.

#### **REFERENCES**

- [1] Giammichele L, Colarossi D, D'Alessandro V, Falone M. Evaluation of the influence of lithium-ion battery composition on thermal power generation. Sustain Energy Fuels 2024;8:1566–1576. [CrossRef]
- [2] Gümüşsu E, Ekici Ö, Köksal M. 3-D CFD modeling and experimental testing of thermal behavior of a Li-Ion battery. Appl Therm Eng 2017;120:484–495.
- [3] Feng X, Ouyang M, Liu X, Lu L, Xia Y, He X. Thermal runaway mechanism of lithium ion battery for electric vehicles: a review. Energy Storage Mater 2018;10:246–267. [CrossRef]
- [4] Maurya M, Gawade S, Zope N. A study of different machine learning algorithms for state of charge estimation in lithium-ion battery pack. Energy Storage 2024;6:e658. [CrossRef]
- [5] Keyser M, Kim GH, Neubauer J, Pesaran A, Santhanagopalan S, Smith K. Design and analysis of large lithium-ion battery systems. Artech; 2014.
- [6] Huang Y, Mei P, Lu Y, Huang R, Yu X, Chena Z, et al. A novel approach for lithium-ion battery thermal management with streamline shape mini channel cooling plates. Appl Therm Eng 2019;157:113623. [CrossRef]
- [7] Zhao Y, Zou B, Li C, Ding Y. Active cooling based battery thermal management using composite phase change materials. Energy Procedia 2019;158:4933–4940. [CrossRef]
- [8] Jilte RD, Kumar R, Ahmadi MH, Chen L. Battery thermal management system employing phase change material with cell-to-cell air cooling. Appl Therm Eng 2019;161:114199. [CrossRef]
- [9] Smith J, Singh R, Hinterberger M, Mochizuki M. Battery thermal management system for electric vehicle using heat pipes. Int J Therm Sci 2018;134:517–529. [CrossRef]
- [10] Cao J, Ling Z, Fang X, Zhang Z. Delayed liquid cooling strategy with phase change material to achieve high temperature uniformity of Li-ion battery under high-rate discharge. J Power Sources 2020;450:227673. [CrossRef]
- [11] Thorat P, Sanap S, Gawade S. A comparative study of thermo-physical properties of different nanofluids for effective heat transfer leading to Li-ion battery pack cooling. Energy Storage 2024;6:1–29. [CrossRef]

- [12] Cracian A, Said U, Winardi S, Madhania S. The thermal characteristics of lithium-ferro-phosphate (LFP) battery pack. AIP Conf Proc 2024;020014.

  [CrossRef]
- [13] Gonder J, Lustbader J, Pesaran A. Thermal management of batteries in advanced vehicles using PCM. Renew Energy 2008;2:134–147. [CrossRef]
- [14] Saw LH, Ye Y, Yew MC, Chong WT, Yew MK, Ng TC. Computational fluid dynamics simulation on open cell aluminium foams for Li-ion battery cooling system. Appl Energy 2017;204:1489–1499. [CrossRef]
- [15] Parsons KK, Mackin TJ. Design and simulation of passive thermal management system for lithium-ion battery packs on an unmanned ground vehicle. J Therm Sci Eng Appl 2017;9:1–9. [CrossRef]
- [16] Qian X, Xuan D, Zhao X, Shi Z. Heat dissipation optimization of lithium-ion battery pack based on neural networks. Appl Therm Eng 2019;162:114289.
- [17] Fan R, Zhang C, Wang Y, Ji C, Meng Z, Xu L, et al. Numerical study on the effects of battery heating in cold climate. J Energy Storage 2019;26:100969. [CrossRef]
- [18] Bai FF, Chen MB, Song WJ, Li Y, Feng ZP, Li Y. Thermal performance of pouch lithium-ion battery module cooled by phase change materials. Energy Proced 2019;158:3682–3689. [CrossRef]
- [19] Jiang L, Zhou L, Li J, Zhang P, Zhou F, Liu Y. LFP battery pack combined heat dissipation strategy structural design. In: 7th Int Conf Energy Electr Power Eng (CEEPE); 2024. p. 1229–1233. [CrossRef]
- [20] KumarSK, MuniamuthuS, Mohan A, Amirthalingam P, Anbu Muthuraja M. Effect of charging and discharging process of PCM with paraffin and Al2O3 additive subjected to three point temperature locations. J Ecol Eng 2022;23:34–42. [CrossRef]
- [21] Thorat P, Sanap S, Gawade S, Patil S. A simulation approach in analyzing performance of fly ash nanofluid for optimizing battery thermal management system used in EVs. Energy Storage 2024;6:e70005.

  [CrossRef]
- [22] Zubairuddin M, Ravi Kumar R, Ali B. Thermomechanical analysis of laser welding of Grade 91 steel. Optik 2021;245:17510. [CrossRef]
- [23] Pavan AR, Arivazhagan B, Zubairuddin M, Vasudevan M. Thermomechanical analysis of A-TIG and MP-TIG welding of 2.25Cr-1Mo steel considering phase transformation. J Mater Eng Perform 2019;28:4903–4917. [CrossRef]
- [24] Zubairuddin M, Albert SK, Mahadevan S, Vasudevan M, Chaudhari V, Suri VK. Numerical simulation of multi-pass GTA welding of Grade 91 steel. J Manuf Process 2017;27:87–97. [CrossRef]
- [25] Nazari A, Farhad S. Heat generation in lithium-ion batteries with different nominal capacities and chemistries. Appl Therm Eng 2017;125:1501–1517. [CrossRef]

- [26] Shen W, Wang N, Zhang J, Wang F, Zhang G. Heat generation and degradation mechanism of lithium-ion batteries during high-temperature aging. ACS Omega 2022;7:44733–44742. [CrossRef]
- [27] Allouhi A, Rehman S. Grid-connected hybrid renewable energy systems for supermarkets with electric vehicle charging platforms: optimization and sensitivity analyses. Energy Rep 2023;9:3305–3318. [CrossRef]
- [28] Zayed ME, Kabeel AE, Shboul B, Ashraf WM, Ghazy M, Irshad K, et al. Performance augmentation and machine learning-based modeling of wavy corrugated solar air collector embedded with thermal energy storage. J Energy Storage 2023;74:109533.

  [CrossRef]
- [29] Ismail NHF, Toha SF, Azubir NAM, Ishak NH, Hassan MK, Ibrahim BSK. Simplified heat generation model for lithium ion battery used in electric vehicle. IOP Conf Ser Mater Sci Eng 2013;53:1–6.

  [CrossRef]
- [30] Kantharaj R, Marconnet AM. Heat generation thermal transport in lithium-ion batteries: a

- scale-bridging perspective. Nanoscale Microscale Thermophys Eng 2019;23:128–156. [CrossRef]
- [31] Zhu S, Han J, Wang YN, Pn TS, Wei YM, Song WL, et al. In-situ heat generation measurement of the anode and cathode in a single-layer lithium ion battery cell. Int J Energy Res 2020;44:9141–9148.

  [CrossRef]
- [32] Chen F, Yu X, Lacarrière B, Le Corre O. Cylindrical lithium-ion battery cells forecast. Energy Procedia 2017;142:4029–4036. [CrossRef]
- [33] Lin C, Ren S. Comparative study on the heat generation behavior of lithium-ion batteries with different cathode materials using accelerating rate calorimetry. Energy Procedia 2017;142:3369–3374. [CrossRef]
- [34] Chauhan VK, Bhattacharya J. Error estimation of Bernardi heat evaluation of Li-ion cells under drive cycle operation. Appl Therm Eng 2024;254:123870.

  [CrossRef]
- [35] Neupane S, Alipanah M, Barnes D, Li X. Heat generation characteristics of LiFePO4 pouch cells with passive thermal management. Energies 2018;11:1243.

  [CrossRef]